

An Improved Exact Riemann Solver for Relativistic Hydrodynamics

By **LUCIANO REZZOLLA**^{1,2} AND **OLINDO ZANOTTI**¹

¹ SISSA, International School for Advanced Studies, Trieste, Italy

² INFN, Department of Physics, Trieste, Italy

(Received 29 October 2018)

A Riemann problem with prescribed initial conditions will produce one of three possible wave patterns corresponding to the propagation of the different discontinuities that will be produced once the system is allowed to relax. In general, when solving the Riemann problem numerically, the determination of the specific wave pattern produced is obtained through some initial guess which can be successively discarded or improved. We here discuss a new procedure, suitable for implementation in an exact Riemann solver in one dimension, which removes the initial ambiguity in the wave pattern. In particular we focus our attention on the relativistic velocity jump between the two initial states and use this to determine, through some analytic conditions, the wave pattern produced by the decay of the initial discontinuity. The exact Riemann problem is then solved by means of calculating the root of a nonlinear equation. Interestingly, in the case of two rarefaction waves, this root can even be found analytically. Our procedure is straightforward to implement numerically and improves the efficiency of numerical codes based on exact Riemann solvers.

1. Introduction

The general Riemann problem is based on the calculation of the one-dimensional temporal evolution of a fluid which, at some given initial time, has two adjacent states characterized by different values of uniform velocity, pressure and density. From a mathematical point of view, the Riemann problem is an initial value problem for a hyperbolic system of partial differential equations, with initial conditions characterized by a discontinuity between the two initial states. These initial conditions establish the way in which the discontinuity will decay after removal of the barrier separating the initial “left” and “right” states. The schematic evolution of a general Riemann problem can be represented as (Martí & Müller 1994)

$$L\mathcal{W}_{\leftarrow}L_*\mathcal{C}R_*\mathcal{W}_{\rightarrow}R, \quad (1.1)$$

where \mathcal{W} denotes a shock or a rarefaction wave that propagates towards the left (\leftarrow) or the right (\rightarrow) with respect to the initial discontinuity, L and R are the known initial left and right states, while L_* and R_* are the new hydrodynamic states that form behind the two waves propagating in opposite directions. These waves are separated by a contact discontinuity \mathcal{C} and therefore have the same values of the pressure and velocity, but different values of the density[†]. The Riemann problem is said to be solved when the velocity, pressure and density in the new states L_* and R_* have been computed, as well as the positions of the waves separating the four states. The solution of the one dimensional Riemann problem in relativistic hydrodynamics was discussed

[†] Note that the contact discontinuity might be also trivial so that the density may not be discontinuous.

in the general case by Martí & Müller (1994) and the reader is referred to their work for further details (see also Pons *et al.* 2000, for the extension to multidimensions).

The numerical solution of a Riemann problem is the fundamental building block of hydrodynamical codes based on Godunov-type finite difference methods. In such methods, the computational domain is discretized and each interface between two adjacent grid-zones is used to construct the initial left and right states of a “local Riemann problem”. The evolution of the hydrodynamical equations is then obtained through the solution across the computational grid of the sequence of local Riemann problems set up at the interfaces between successive grid-zones (see Martí & Müller 1996, but also Godunov 1959 and Colella & Woodward 1984). The “core” of each of these local Riemann problems consists of determining the fluid pressure across the contact discontinuity, which can be calculated by imposing the continuity of the normal component of the fluid velocity across \mathcal{C}

$$v_{L_*}(p_*) = v_{R_*}(p_*). \quad (1.2)$$

In general, (1.2) is a nonlinear algebraic equation in the unknown pressure p_* and requires a numerical solution. Depending on the different wave patterns forming after the decay of the discontinuity, a different nonlinear equation will need to be solved[†]. This initial “ambiguity” in the wave pattern produced corresponds to the fact that the interval in pressure bracketing the solution p_* is not known a priori. In practice this lack of information is compensated by the use of efficient numerical algorithms which, via a process of trial and error, determine the correct wave pattern and then proceed to the solution of the corresponding nonlinear equation (Martí, & Müller 1999).

In this paper, we show that the relativistic expression for the relative velocity between the two initial states is a function of the unknown pressure p_* and so a new procedure for numerically solving the exact Riemann problem can be proposed in which the pressure p_* is no longer obtained by the solution of equation (1.2). Rather, p_* is calculated by equating the relativistic invariant expression for the relative velocity between the two initial states with the value given by the initial conditions.

When compared to equivalent approaches, our exact Riemann solver has some advantages. Firstly, we can remove the ambiguity mentioned above and determine the generated flow pattern by simply comparing the relative velocity between the two initial states with reference values built from the initial conditions of the Riemann problem. Doing so provides immediate information about which of the nonlinear equations (one for every wave pattern) needs to be solved. Secondly, by knowing the wave pattern we can produce an immediate bracketing of the solution. Doing so gives improved efficiency in the numerical root finding procedure. Finally, for one of the wave patterns (i.e. for two rarefaction waves moving in opposite directions) our method provides the solution of the relativistic Riemann problem in a closed analytic form.

Because of its simplicity, the numerical implementation of our method is straightforward and can be accomplished with a much smaller number of lines of code. When compared with other exact Riemann solvers (e. g. Martí & Müller 1999) it has also proved to be computationally more efficient. In particular, when solving a generic hydrodynamical problem (in which one solves for very simple Riemann problems) the approach proposed here brackets the solution very closely and this produces substantial computational improvements of up to 30%. For the cases discussed here however, where very strong shocks are considered, the speed-up is below 10%.

This paper briefly introduces our idea and is organized as follows: in Section 2 we define the mathematical set-up for the formulation of the Riemann problem in relativistic hydrodynamics.

[†] This approach is usually referred to as an “exact” Riemann solver to distinguish it from the family of so called “approximate” Riemann solvers, where the system of equations to be solved is reduced to quasi-linear form, thus avoiding any iterative procedure. See, for example, the approximate Riemann solver of Roe (1981).

In Section 3 we determine the basic relativistic expressions linking the velocities ahead of and behind a shock or a rarefaction wave. These expressions will be used repeatedly in the following Sections 4–6, where we will write explicit criteria for the occurrence of the three possible wave patterns. Section 7 discusses how the criteria can be used for making an efficient numerical implementation of a Riemann solver and briefly presents a comparison of performances with more traditional algorithms. Finally, Section 8 presents our conclusions. Throughout, we use a system of units in which $c = 1$.

2. Setting up the Relativistic Riemann Problem

Consider a perfect fluid with four-velocity $u^\mu = W(1, v, 0, 0)$ with $W \equiv (1 - v^2)^{-1/2}$ being the Lorentz factor and with a stress-energy tensor

$$T^{\mu\nu} = (e + p)u^\mu u^\nu + p\eta^{\mu\nu} = \rho h u^\mu u^\nu + p\eta^{\mu\nu}, \quad (2.1)$$

where $\mu = 0, \dots, 3$, $\eta^{\mu\nu} = \text{diag}(-1, 1, 1, 1)$ and e, p are the proper energy density and pressure, respectively. Assume moreover that the fluid obeys a polytropic equation of state

$$p = k(s)\rho^\gamma = (\gamma - 1)\rho\epsilon, \quad (2.2)$$

where ρ is the proper rest mass density, γ is the adiabatic index, and $k(s)$ is the polytropic constant, dependent only on the specific entropy s (the latter is generally assumed to be different in the two initial states). Straightforward expressions can be written relating e and p to the specific enthalpy h and to the specific internal energy ϵ of the fluid

$$e = \rho(1 + \epsilon) = \rho + \frac{p}{\gamma - 1}, \quad (2.3)$$

$$h = 1 + \epsilon + \frac{p}{\rho} = 1 + \frac{p}{\rho} \left(\frac{\gamma}{\gamma - 1} \right). \quad (2.4)$$

Consider now the fluid to consist of an initial left state (indicated with an index 1) and an initial right state (indicated with an index 2), each having prescribed and different values of uniform pressure, density and velocity[†]. The discontinuity between the two states which has been constructed in this way will then decay producing one of the three wave patterns listed below

(i) *two shock waves*, one moving towards the initial left state, and the other towards the initial right state: $LS_{\leftarrow}L_*CR_*S_{\rightarrow}R$.

(ii) *one shock wave and one rarefaction wave*, the shock moving towards the initial right state, and the rarefaction towards the initial left state (or viceversa if $p_2 > p_1$): $LR_{\leftarrow}L_*CR_*S_{\rightarrow}R$.

(iii) *two rarefaction waves*, one moving towards the initial left state, and the other towards the initial right state: $LR_{\leftarrow}L_*CR_*R_{\rightarrow}R$. A special case of this wave pattern is produced when the two rarefaction waves leave a vacuum region behind them.

The basis of our approach lies in the possibility of determining “a priori” which of these three wave patterns will actually result by simply comparing the value of the special relativistic relative velocity between the initial left and right states

$$v_{12} \equiv \frac{v_1 - v_2}{1 - v_1 v_2}, \quad (2.5)$$

with the values of the limiting relative velocities for the occurrence of the wave patterns (i)–(iii).

[†] Note that hereafter we will consider the fluid to be of the same type in the two initial states. In principle, in fact, the fluid in the two initial states might be governed by two different equations of state or by polytropic equations of state with different polytropic indices. The formulation of the problem in that case is equivalent to the one presented here for a single type of fluid but particular attention must be paid to distinguishing the different components in the relevant expressions.

In this respect, our approach represents the relativistic generalization of a similar analysis proposed in Newtonian hydrodynamics by Landau and Lifshitz (1987) (see also Gheller 1997 for a numerical implementation). Mathematically, the occurrence of the different cases can be distinguished because the relative velocity[‡] (2.5) is a continuous monotonic function of the pressure p_* across the contact discontinuity. This is shown in Fig. 1 where we have plotted v_{12} as a function of p_* and it is proved mathematically in Appendix A. Note that the curve shown in Fig. 1 is effectively produced by the continuous joining of three different curves describing the relativistic relative velocity for the three different wave patterns corresponding respectively to two shocks (2S, indicated as a dashed line), one shock and one rarefaction wave (SR, indicated as a dotted line), and two rarefaction waves (2R, indicated as a continuous line). The joining of the different curves occurs at precise values of the relative velocity which we have indicated as $(\tilde{v}_{12})_{2S}$, $(\tilde{v}_{12})_{SR}$, $(\tilde{v}_{12})_{2R}$ and which depend uniquely on the initial conditions of the two unperturbed states. These three values of the relative velocity mark the extremes of three different intervals on the vertical axis and correspond to the three different cases (i)–(iii).

Within this framework then, it is sufficient to compare the relative velocity between the initial states (2.5) with the calculated values of the limiting relative velocities $(\tilde{v}_{12})_{2S}$, $(\tilde{v}_{12})_{SR}$, $(\tilde{v}_{12})_{2R}$, to determine, in advance, which wave pattern will be produced. This, in turn, determines the correct equation to solve and the correct bracketing of the solution. In the following Sections we will discuss in detail how to derive analytic expressions for the limiting relative velocities and use them efficiently within a numerical code.

3. Limiting Relative Velocities: Fundamental Expressions

The expression for the relative velocity (2.5) is a relativistic invariant, but its calculation can be considerably simplified when performed in an appropriate reference frame. In practice, we will consider each of the three wave patterns (i)–(iii) as being composed of two “discontinuity fronts” (two shocks, two rarefaction waves, or one of each) moving in opposite directions and separated by a region where a contact discontinuity is present. In the case of a shock, in particular, it is useful to use a reference frame comoving with the shock front, in which the relativistic expression for the relative velocities ahead of (a) and behind (b) the shock takes the form (Taub 1978)

$$v_{ab} \equiv \frac{v_a - v_b}{1 - v_a v_b} = \sqrt{\frac{(p_b - p_a)(e_b - e_a)}{(e_a + p_b)(e_b + p_a)}}. \quad (3.1)$$

In the case of a rarefaction wave, on the other hand, it is more convenient to use the Eulerian frame in which the initial states are measured and which has one of the axes aligned with the direction of propagation of the wave front. In such a frame, the flow velocity at the back of a rarefaction wave (i.e. behind the tail of the rarefaction wave) can be expressed as a function of pressure at the back of the wave as

$$v_b = \frac{(1 + v_a)A_{\pm}(p_b) - (1 - v_a)}{(1 + v_a)A_{\pm}(p_b) + (1 - v_a)}. \quad (3.2)$$

The quantity $A_{\pm}(p)$ in (3.2) is defined as (Martí & Müller 1994)

$$A_{\pm}(p) \equiv \left\{ \left[\frac{(\gamma - 1)^{1/2} - c_s(p)}{(\gamma - 1)^{1/2} + c_s(p)} \right] \left[\frac{(\gamma - 1)^{1/2} + c_s(p_a)}{(\gamma - 1)^{1/2} - c_s(p_a)} \right] \right\}^{\pm 2/(\gamma - 1)^{1/2}}, \quad (3.3)$$

with the \pm signs corresponding to rarefaction waves propagating to the left (\mathcal{R}_{\leftarrow}) and to the right ($\mathcal{R}_{\rightarrow}$) of the contact discontinuity, respectively. The quantity $c_s(p)$ in (3.3) is the local

[‡] For compactness we will hereafter refer to as “relative velocity” the relativistic invariant expression.

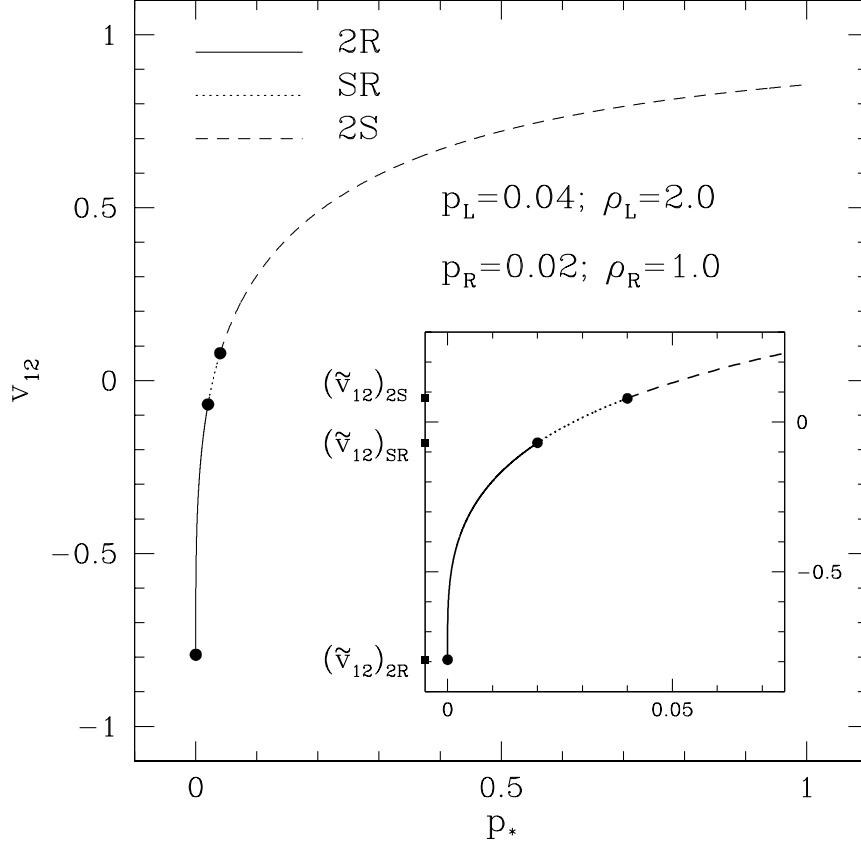


FIGURE 1. Relative velocity between the two initial states 1 and 2 as a function of the pressure at the contact discontinuity. Note that the curve shown is given by the continuous joining of three different curves describing the relative velocity corresponding respectively to two shocks (a dashed line), one shock and one rarefaction wave (dotted line), and two rarefaction waves (continuous line). The joining of the curves is indicated with filled dots. The small inset on the right shows a magnification for a smaller range of p_* and we have indicated with filled squares the limiting values for the relative velocities $(\tilde{v}_{12})_{2S}$, $(\tilde{v}_{12})_{SR}$, $(\tilde{v}_{12})_{2R}$

sound speed which, for a polytropic equation of state, can be written as

$$c_s = \sqrt{\frac{\gamma(\gamma-1)p}{(\gamma-1)\rho + \gamma p}}. \quad (3.4)$$

We can now use expression (3.2) to write an invariant expression for the relative velocity across a rarefaction wave (i.e. the relative velocity of the fluid ahead of the rarefaction wave and behind the tail of the rarefaction wave) as

$$v_{ab} = \frac{1 - A_{\pm}(p_b)}{1 + A_{\pm}(p_b)}. \quad (3.5)$$

Expressions (3.1) and (3.5) are not yet in a useful form since they cannot be combined to give (2.5). However, we can exploit the fact they are relativistic invariants to evaluate them in the rest frame of the contact discontinuity. The latter is, by definition, comoving with the fluid behind

the discontinuity fronts and within such a frame we can set $v_b = 0$ and use equations (3.1), (3.5) to obtain an explicit expression for the velocity ahead of the wave front. The expressions for the velocities ahead of both discontinuity fronts obtained in this way can then be combined so as to evaluate expression (2.5).

In the following Sections we will apply the procedure outlined above to derive the relative velocity between the left and right states for the three different wave patterns (i)–(iii). We will denote with indices 3 and 3' the quantities evaluated in the left (L_*) and right (R_*) states behind the discontinuity fronts, and where $p_3 = p_{3'}$, $v_3 = v_{3'}$, and $\rho_3 \neq \rho_{3'}$. Note also that in all of the different cases we will assume that $p_1 > p_2$, and take the positive x -direction as being the one from the region 1 to the region 2 (An alternative opposite choice is also possible.).

4. $LS_{\leftarrow}L_*CR_*S_{\rightarrow}R$: Two Shock Fronts

We start by considering the wave pattern produced by two shocks propagating in opposite directions (see Fig. 2). This situation is characterized by a value of the pressure downstream of the shocks which is larger than the pressures in the unperturbed states, i.e. $p_3 > p_1 > p_2$. Applying equation (3.1) to the shock front moving towards the left and evaluating it in the reference frame of the contact discontinuity, we can write the velocity ahead of the left propagating shock as

$$v_1 = \sqrt{\frac{(p_3 - p_1)(e_3 - e_1)}{(e_1 + p_3)(e_3 + p_1)}}. \quad (4.1)$$

Similarly, we can apply equation (3.1) to the shock front moving towards the right and evaluate it in the frame comoving with the contact discontinuity to obtain that the velocity ahead of the right propagating shock is

$$v_2 = -\sqrt{\frac{(p_3 - p_2)(e_{3'} - e_2)}{(e_2 + p_3)(e_{3'} + p_2)}}. \quad (4.2)$$

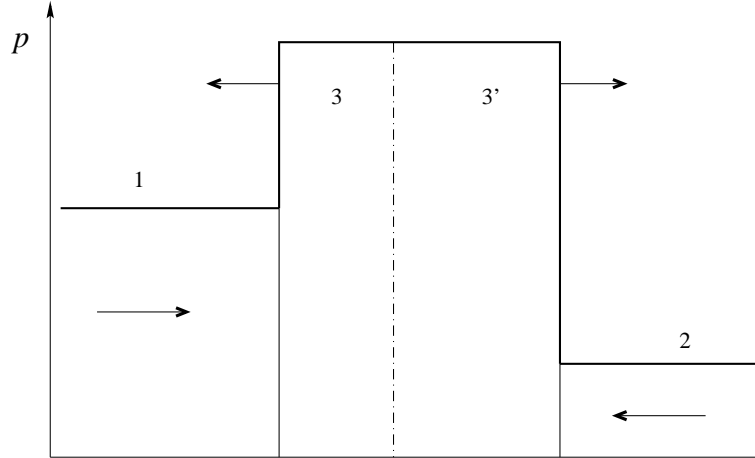


FIGURE 2. Schematic wave pattern in the pressure for the decay of a discontinuity generating two shock waves propagating in opposite directions. The vertical solid lines show the position of the shock fronts while the dot-dashed vertical line shows the position of the contact discontinuity. The different arrows show the gas flow and the directions of propagation of the different fronts.

Equations (4.1) and (4.2) can now be used to derive the relativistic expression for the relative velocity of the flow ahead of the two shocks $(v_{12})_{2S}$. As proved in Appendix A, the expression

for the relative velocity between the unperturbed states is a monotonic function of p_3 for all possible wave patterns. In particular, for the present choice of initial data, this expression is a monotonically increasing function of p_3 . As a result, the value of $(v_{12})_{2S}$ can be used to build a criterion for the occurrence of two shocks propagating in opposite directions. In fact, since p_1 is the smallest value that p_3 can take, two shocks will form if

$$v_{12} > (\tilde{v}_{12})_{2S} \equiv \sqrt{\frac{(p_1 - p_2)(\hat{e} - e_2)}{(\hat{e} + p_2)(e_2 + p_1)}}, \quad (4.3)$$

where

$$\hat{e} = \hat{h}\hat{\rho} - p_1 = \hat{h} \frac{\gamma p_1}{(\gamma - 1)(\hat{h} - 1)} - p_1, \quad (4.4)$$

and \hat{h} is the only positive root of the Taub adiabat (Taub 1978, Martí & Müller 1994)

$$\left[1 + \frac{(\gamma - 1)(p_2 - p_3)}{\gamma p_3}\right] \hat{h}^2 - \frac{(\gamma - 1)(p_2 - p_3)}{\gamma p_3} \hat{h} + \frac{h_2(p_2 - p_3)}{\rho_2} - h_2^2 = 0. \quad (4.5)$$

when $p_3 \rightarrow p_1$. Simple calculations reported in Appendix B show that the Newtonian limit of $(\tilde{v}_{12})_{2S}$ corresponds to the expression derived by Landau and Lifshitz (1987).

5. $LS_{\leftarrow}L_*CR_*\mathcal{R}_{\rightarrow}R$: One Shock and one Rarefaction Wave

We next consider the wave pattern produced by one shock front propagating towards the right and one rarefaction wave propagating in the opposite direction (see Fig. 3). This situation is therefore characterized by $p_1 > p_3 > p_2$.

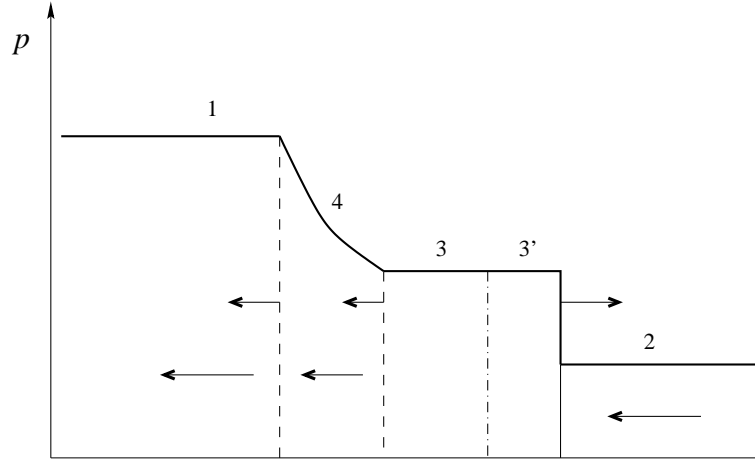


FIGURE 3. Schematic wave pattern in the pressure for the decay of the discontinuity into a shock wave propagating towards the right and a rarefaction wave propagating in the opposite direction. The vertical lines show the discontinuities formed (continuous for the shock front; dashed for the head and the tail of the rarefaction wave; dot-dashed for the contact discontinuity) while the arrows show their direction of propagation and that of the gas flow.

Evaluating expression (3.5) in the reference frame comoving with the contact discontinuity, we can evaluate the flow velocity ahead of the rarefaction wave to be

$$v_1 = \frac{1 - A_+(p_3)}{1 + A_+(p_3)}, \quad (5.1)$$

where

$$A_+(p_3) \equiv \left\{ \left[\frac{(\gamma - 1)^{1/2} - c_s(p_3)}{(\gamma - 1)^{1/2} + c_s(p_3)} \right] \left[\frac{(\gamma - 1)^{1/2} + c_s(p_1)}{(\gamma - 1)^{1/2} - c_s(p_1)} \right] \right\}^{2/(\gamma-1)^{1/2}}. \quad (5.2)$$

The flow velocity ahead of the shock front can be derived as in Section 4 by evaluating equation (3.1) in the reference frame of the contact discontinuity to get

$$v_2 = -\sqrt{\frac{(p_3 - p_2)(e_{3'} - e_2)}{(e_{3'} + p_2)(e_2 + p_3)}}, \quad (5.3)$$

which, combined with expression (5.1), can be used to derive the relativistic expression for the relative velocity of the fluids ahead of the shock and ahead of the rarefaction wave $(v_{12})_{SR}$. As for $(v_{12})_{2S}$, it can be shown that $(v_{12})_{SR}$ is a monotonically increasing function of p_3 (see Fig. 1 and Appendix A for an analytic proof). Exploiting now the knowledge that for this wave pattern the pressure in the region between the two waves must satisfy $p_2 < p_3 < p_1$, we can establish that the criterion on the relative velocity for having one shock and one rarefaction wave is

$$(\tilde{v}_{12})_{SR} = \left. \frac{1 - A_+(p_3)}{1 + A_+(p_3)} \right|_{p_3=p_2} < v_{12} \leq \sqrt{\frac{(p_1 - p_2)(\hat{e} - e_2)}{(e_2 + p_1)(\hat{e} + p_2)}} = (\tilde{v}_{12})_{2S}. \quad (5.4)$$

Note that the upper limit of (5.4) coincides with $(\tilde{v}_{12})_{2S}$, which is the lower limit for the occurrence of 2 shock waves (4.3) and whose Newtonian limit coincides with the equivalent one found by Landau and Lifshitz (1987) (see Appendix B). Note also that in the limit, $p_3 \rightarrow p_2$, regions 1 and 2 are connected by a single rarefaction wave. In this case the sound speed can be computed using $p_3 = p_2$ but with $\rho_3 = \rho_1(p_2/p_1)^{1/\gamma}$. Finally, note that this is the only wave pattern in which v_1 and v_2 have the same sign and it therefore includes the classical *shock-tube problem*, where $v_1 = v_2 = 0$.

6. $L\mathcal{R}_\leftarrow L_*CR_*\mathcal{R}_\rightarrow R$: Two Rarefaction Waves

We now consider the wave pattern produced by two rarefaction waves propagating in opposite directions (see Fig. 4). This situation is characterized by $p_1 > p_2 > p_3$ and when the waves are sufficiently strong it might lead to a vacuum region ($\rho_3 = 0$) behind the rarefaction waves.

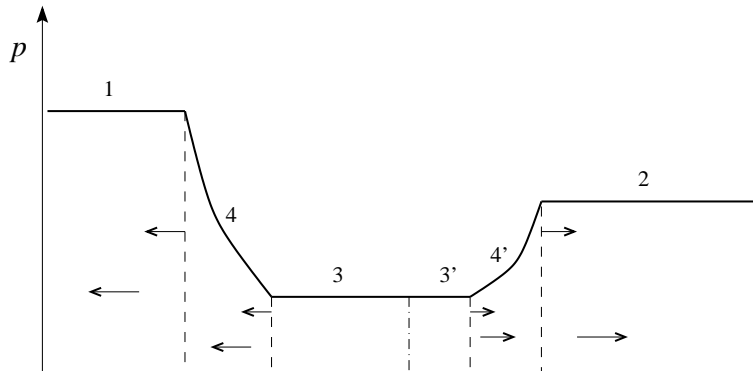


FIGURE 4. Schematic wave pattern in the pressure for the decay of the discontinuity into two rarefaction waves propagating in opposite directions. The vertical lines show the discontinuities formed (dashed for the head and the tail of the rarefaction waves; dot-dashed for the contact discontinuity) while the arrows show their direction of propagation and that of the gas flow. Note that the region downstream of the two rarefaction waves has a density $\rho_3 > 0$.

Following again the same procedure discussed in the previous Section, we can determine the values of the fluid velocities ahead of the two rarefaction waves as, respectively,

$$v_1 = -\frac{A_+(p_3) - 1}{A_+(p_3) + 1}, \quad (6.1)$$

$$v_2 = \frac{1 - A_-(p_{3'})}{1 + A_-(p_{3'})}, \quad (6.2)$$

where

$$A_-(p_{3'}) \equiv \left\{ \left[\frac{(\gamma - 1)^{1/2} - c_s(p_{3'})}{(\gamma - 1)^{1/2} + c_s(p_{3'})} \right] \left[\frac{(\gamma - 1)^{1/2} + c_s(p_2)}{(\gamma - 1)^{1/2} - c_s(p_2)} \right] \right\}^{-2/(\gamma-1)^{1/2}}. \quad (6.3)$$

We have indicated with $c_s(p_{3'})$ the sound speed in the region $3'$, which differs from the one in region 3 because of the jump in the densities ρ_3 and $\rho_{3'}$. The relative velocity built using (6.1) and (6.2) is then

$$(v_{12})_{2R} = -\frac{A_+(p_3) - A_-(p_{3'})}{A_+(p_3) + A_-(p_{3'})}. \quad (6.4)$$

As for the relative velocities of the previous wave patterns, it can be shown that $(v_{12})_{2R}$ is a monotonically increasing function of p_3 (see Fig. 1 and Appendix A for an analytic proof) so that the criterion for the occurrence of two rarefaction waves can be expressed as

$$(v_{12})_{2R} \Big|_{p_3=0} < v_{12} \leq (v_{12})_{2R} \Big|_{p_3=p_2} = (\tilde{v}_{12})_{SR}, \quad (6.5)$$

where $A_-(p_3 = p_2) = 1$ and therefore the upper limit for (6.5) coincides with the lower limit for (5.4).

The condition (6.5) can also be expressed in a more useful form as

$$-\frac{S_1 - S_2}{S_1 + S_2} < v_{12} \leq -\frac{1 - A_+(p_2)}{1 + A_+(p_2)}, \quad (6.6)$$

where, the constants S_1 and S_2 are shorthand for

$$S_1 \equiv \left[\frac{(\gamma - 1)^{1/2} + c_s(p_1)}{(\gamma - 1)^{1/2} - c_s(p_1)} \right]^{2/(\gamma-1)^{1/2}} \quad (6.7)$$

$$S_2 \equiv \left[\frac{(\gamma - 1)^{1/2} + c_s(p_2)}{(\gamma - 1)^{1/2} - c_s(p_2)} \right]^{-2/(\gamma-1)^{1/2}}. \quad (6.8)$$

An important property of equation (6.4) is that it can be inverted analytically. This involves rewriting it in terms of a quartic equation in the unknown sound speed in the region L_* (see Appendix C for the explicit form of the equation). Once the relevant real root of this equation has been calculated analytically, the value of the pressure p_* can be found through a simple algebraic expression. In this case, therefore, the solution of the exact relativistic Riemann problem can be found in an analytic closed form.

We conclude the analysis of the different wave patterns with a comment on the case of two rarefaction waves propagating in opposite directions and leaving behind them a region with zero density and pressure. This situation occurs when the fluids in the regions 1 and 2 are moving sufficiently fast in opposite directions. This is the case whenever the relative velocity between the two states ahead of the rarefaction waves is less than or equal to the lower limit for $(v_{12})_{2R}$, i.e.

$$v_{12} \leq (\tilde{v}_{12})_{2R} \equiv -\frac{S_1 - S_2}{S_1 + S_2}. \quad (6.9)$$

Also in this case, taking the Newtonian limit of $(\tilde{v}_{12})_{2R}$ we obtain the corresponding expression derived by Landau and Lifshitz (1987) (see Appendix B). Finally, note that when a vacuum is produced, v_{12} is no longer dependent on p_3 and this branch of the curve cannot be plotted in Fig.1.

7. Numerical Implementation

The core of most exact Riemann solvers, in both Newtonian and relativistic hydrodynamics, is based on the numerical computation of the pressure in the regions L_* and R_* that form behind the waves. The key property exploited when performing the numerical calculation is that the velocity in such regions can be expressed as a monotonic function of the pressure i.e. $v_{L_*} = v_{L_*}(p_{L_*})$, and $v_{R_*} = v_{R_*}(p_{R_*})$. Since there is no jump across a contact discontinuity in either the velocity or in the pressure, the numerical solution of the Riemann problem consists then of finding the root $p_* = p_{L_*} = p_{R_*}$ of the nonlinear equation

$$v_{L_*}(p_*) - v_{R_*}(p_*) = 0, \quad (7.1)$$

where v_{L_*}, v_{R_*} have different functional forms according to the different wave patterns produced. This method has two obvious disadvantages: (1) it cannot determine, using the initial conditions, the wave pattern produced and thus which of the functional forms to use for v_{L_*}, v_{R_*} ; (2) it cannot provide a straightforward bracketing interval for the root. In practice, however, these difficulties are effectively balanced by efficient algorithms based on a sequence of trial and error attempts that rapidly bracket the root and determine the correct equation to solve (see, for instance, Martí, & Müller 1999 and the algorithm presented therein).

The exact Riemann solver which we propose here differs from the one discussed above mostly because it avoids the disadvantages (1) and (2). In fact, as discussed in Section 1, by comparing the relative velocity between the initial left and right states $(v_{12})_0$ with the relevant limiting values constructed from the initial conditions $(\tilde{v}_{12})_{2S}, (\tilde{v}_{12})_{SR}, (\tilde{v}_{12})_{2R}$, we can determine both the wave pattern which will be produced and the correct bracketing range in the pressure. Once this information has been obtained, the Riemann problem can be solved either through the solution of equation (7.1) or, equivalently, by looking for the value of the pressure p_* which would produce a relative velocity $(v_{12})_0$. This latter approach, which we will be discussing in the following, involves then the solution of the nonlinear equation

$$v_{12}(p_*) - (v_{12})_0 = 0, \quad (7.2)$$

where $v_{12}(p_*)$ is given by the expressions for $(v_{12})_{2S}$, or $(v_{12})_{SR}$, or $(v_{12})_{2R}$ derived in Sections 4–6. Furthermore, in the case of two rarefaction waves, equation (7.2) can also be solved analytically.

Besides providing direct information about the wave pattern produced, about the correct equation to solve and the relevant bracketing interval, our approach is also very simple to implement numerically. In practice, the basic steps for the solution of the Riemann problem can be summarised as follows:

- (a) Evaluate from the initial conditions the three limiting relative velocities $(\tilde{v}_{12})_{2S}, (\tilde{v}_{12})_{SR}, (\tilde{v}_{12})_{2R}$.
- (b) Determine the wave pattern and the functional form of $v_{12}(p_*)$ by comparing $(v_{12})_0$ with the limiting values calculated in (a) and according to the scheme below.

$$\begin{array}{ll}
(v_{12})_0 > (\tilde{v}_{12})_{2S}: & \mathcal{S}_{\leftarrow} \mathcal{C} \mathcal{S}_{\rightarrow}, & v_{12}(p_*) = (v_{12})_{2S} \\
(\tilde{v}_{12})_{SR} < (v_{12})_0 \leq (\tilde{v}_{12})_{2S}: & L \mathcal{R}_{\leftarrow} L_* \mathcal{C} R_* \mathcal{S}_{\rightarrow} R, & v_{12}(p_*) = (v_{12})_{SR} \\
(\tilde{v}_{12})_{2R} < (v_{12})_0 \leq (\tilde{v}_{12})_{SR}: & L \mathcal{R}_{\leftarrow} L_* \mathcal{C} R_* \mathcal{R}_{\rightarrow} R, & v_{12}(p_*) = (v_{12})_{2R} \\
(v_{12})_0 \leq (\tilde{v}_{12})_{2R}: & L \mathcal{R}_{\leftarrow} L_* \mathcal{C} R_* \mathcal{R}_{\rightarrow} R \text{ with vacuum}, & -
\end{array}$$

(c) According to the wave pattern found, determine the extremes p_{max} and p_{min} of the pressure interval bracketing p_* . Within our conventions this is equivalent to setting[†]

	$\mathcal{S}_{\leftarrow} \mathcal{C} \mathcal{S}_{\rightarrow}$	$L \mathcal{R}_{\leftarrow} L_* \mathcal{C} R_* \mathcal{S}_{\rightarrow} R$	$L \mathcal{R}_{\leftarrow} L_* \mathcal{C} R_* \mathcal{R}_{\rightarrow} R$
p_{min}	$\max(p_1, p_2)$	$\min(p_1, p_2)$	0
p_{max}	∞	$\max(p_1, p_2)$	$\min(p_1, p_2)$

(d) Solve equation (7.2) and determine p_* .

(e) Complete the solution of the Riemann problem by computing the remaining variables of the intermediate states L_* and R_* .

We have implemented our algorithm for an exact Riemann solver and have tested it for a range of Riemann problems. We have also compared the performance of our algorithm with the “standard” approach presented by Martí & Müller 1999 and have found a systematic reduction in the computational costs for the same level of accuracy in the solution. The quantitative efficiency improvement depends on the type of problem under consideration. In the case of a generic hydrodynamical problem (in which very simple Riemann problems are solved), our approach brackets the solution very closely and this produces substantial computational improvements of up to 30%. However, for the specific cases discussed in this paper, where very strong shocks have been considered, the speed-up is smaller and of the order of 10%. It is worth noting that such an improvement could reduce appreciably the computational costs in three-dimensional relativistic hydrodynamics codes, where this operation is repeated a very large number of times.

8. Conclusion

We have presented a new procedure for the numerical solution of the exact Riemann problem in relativistic hydrodynamics. In this approach special attention is paid to the relativistic invariant expression for the relative velocity v_{12} between the unperturbed left and right states. This has been shown to be a monotonic function of the pressure p_* in the region formed between the wave fronts. The determination of this pressure is the basic step in the solution of the exact Riemann problem.

The use of the relative velocity has a number of advantages over alternative exact Riemann solvers discussed in the literature. In particular, it extracts the information implicitly contained in the data for two initial states to deduce the wave pattern that will be produced by the decay of the discontinuity between these two states. This, in turn, allows an “a priori” determination to be made of the interval in pressure bracketing p_* and the correct functional form for the nonlinear

[†] Note that in practice, the upper limit for the pressure in the case of two shocks is found by starting from a reasonable value above p_{min} , which is incremented until the solution is effectively bracketed.

equation whose root will solve the exact Riemann problem. All of these advantages translate, in practice, into a simpler algorithm to implement and an improved efficiency in the numerical solution of the Riemann problem. Furthermore, in the case of two rarefaction waves propagating in opposite directions (and in strict analogy with what happens in Newtonian hydrodynamics), the use of the relative velocity allows for the solution of the Riemann problem in an analytic closed form.

Because of all of the advantages discussed above, its intrinsic simplicity of implementation and the numerical efficiency gain it produces, this new exact Riemann solver should be considered as an interesting alternative to the traditional exact Riemann solver presently discussed in the literature. Investigations about the extension of this approach to multidimensions are currently in progress.

It is a pleasure to thank J. A. Font, C. Gheller, and J. C. Miller for useful discussions. Financial support for this research has been provided by the Italian Ministero dell'Università e della Ricerca Scientifica and by the EU Programme 'Improving the Human Research Potential and the Socio-Economic Knowledge Base' (Research Training Network Contract HPRN-CT-2000-00137)."

Appendix A: Monotonicity of the relative velocity as function of p_*

We here prove that v_{12} is a monotonic function of p_* for all of the possible wave patterns. In particular, because of our choice of referring the initial left state as to "1" and the initial right state as to "2", we will here show that v_{12} is a monotonically *increasing* function of p_* .

Denoting by a' the first derivative of the quantity a with respect to $p_* = p_3 = p_{3'}$, it is straightforward to obtain that the first derivative of (2.5) is

$$v'_{12} = \frac{v'_1(1 - v_2^2) - v'_2(1 - v_1^2)}{(1 - v_1 v_2)^2}. \quad (8.1)$$

Since $v_1 \leq 1$, $v_2 \leq 1$, the two terms in the parentheses of (8.1) are always positive, and the proof that v_{12} is monotonically increasing will follow if it can be shown that v'_1 and $-v'_2$ are both positive. We will do so for each of the three possible wave patterns.

Two Shock Fronts

Taking the derivative of the fluid velocity ahead of the left propagating shock front (measured from the contact discontinuity) [cf. equation (4.1)] we obtain

$$v'_1 = \frac{(e_1 + p_1) [(e_3 - e_1)(e_3 + p_1) + (p_3 - p_1)(e_1 + p_3)e'_3]}{2v_1(e_1 + p_3)^2(e_3 + p_1)^2}. \quad (8.2)$$

Since the energy density is an increasing function of pressure, $e'_3 > 0$; furthermore, $p_3 \geq p_1$ and $e_3 \geq e_1$ for the wave pattern considered and $v'_1 > 0$ as a result. The equivalent expression for the derivative of the fluid velocity ahead of the right propagating shock front (measured from the contact discontinuity) [cf. eq (4.2)] can be obtained by replacing in equation (8.2) the indices 1 and 3 by 2 and 3' respectively, i.e.

$$v'_2 = \frac{(e_2 + p_2) [(e_{3'} - e_2)(e_{3'} + p_2) + (p_{3'} - p_2)(e_2 + p_{3'})e'_{3'}]}{2v_2(e_2 + p_{3'})^2(e_{3'} + p_2)^2}. \quad (8.3)$$

Since now for the wave pattern considered: $v_2 < 0$, $p_{3'} \geq p_2$ and $e_{3'} \geq e_2$, we are led to conclude that $-v'_2 > 0$, thus making the overall v'_{12} positive for any value of p_3 .

One Shock and one Rarefaction Wave

In this case we only need to show that $v'_1 > 0$ since for the velocity ahead of the right propagating shock front we can use the results derived in (8.3). Taking the derivative of expression (5.1) then yields

$$v'_1 = -\frac{2A'_+(p_3)}{[1 + A_+(p_3)]^2}, \quad (8.4)$$

where

$$\begin{aligned} A'_+(p_3) &= -4 \left| \frac{(\gamma - 1)^{1/2} + c_s(p_1)}{(\gamma - 1)^{1/2} - c_s(p_1)} \right| \frac{A_+(p_3)^{(2-\sqrt{\gamma-1})/2}}{[(\gamma - 1)^{1/2} + c_s(p_3)]^2} c'_s(p_3) \\ &\equiv -C_1 c'_s(p_3), \end{aligned} \quad (8.5)$$

where $C_1 > 0$. When the sound speed $c_s(p_3)$ is an increasing function of pressure, as is the case for a polytropic equation of state [cf. eq (2.2)], $v'_1 > 0$ and therefore $v'_{12} > 0$.

Two Rarefaction Waves

What we need to show in this case is that $v'_2 < 0$ since we can exploit the previous result that $v'_1 > 0$ where v_1 is the fluid velocity ahead of the left propagating rarefaction wave as measured from the contact discontinuity. In this case, taking the derivative of expression (6.2) one obtains

$$v'_2 = -\frac{2A'_-(p_{3'})}{[1 + A_-(p_{3'})]^2}, \quad (8.6)$$

where now

$$\begin{aligned} A'_-(p_{3'}) &= 4 \left| \frac{(\gamma - 1)^{1/2} + c_s(p_2)}{(\gamma - 1)^{1/2} - c_s(p_2)} \right| \frac{A_-(p_{3'})^{(2+\sqrt{\gamma-1})/2}}{[(\gamma - 1)^{1/2} + c_s(p_{3'})]^2} c'_s(p_{3'}) \\ &\equiv C_2 c'_s(p_{3'}) \end{aligned} \quad (8.7)$$

with $C_2 > 0$ and therefore $v'_2 < 0$.

We have therefore shown that for all of the wave patterns considered $v'_1 > 0$ and $-v'_2 > 0$, thus proving that v_{12} is always a monotonically increasing function of p_* .

Appendix B: Newtonian limits of $(\tilde{v}_{12})_{2S}$, $(\tilde{v}_{12})_{SR}$, $(\tilde{v}_{12})_{2R}$

We here show that the three limiting values of $(\tilde{v}_{12})_{2S}$, $(\tilde{v}_{12})_{SR}$ and $(\tilde{v}_{12})_{2R}$ reduce to their Newtonian counterparts in the limit of $v, c_s \rightarrow 0$, and $h \rightarrow 1$. In particular, we will restrict ourselves to considering the case of a polytropic equation of state (2.2).

We start by considering the Newtonian limit of $(\tilde{v}_{12})_{2S}$ which is obtained when $p/e \ll 1$ and $e \rightarrow 1/V$, with $V = 1/\rho$ being the specific volume. In this case, then

$$\begin{aligned} (\tilde{v}_{12})_{2S} \Big|_{\text{Newt}} &= \sqrt{\frac{(p_1 - p_2)(\hat{e} - e_2)}{\hat{e}e_2}} \\ &= \sqrt{(p_1 - p_2)(1/e_2 - 1/\hat{e})}. \end{aligned} \quad (8.1)$$

which coincides with the corresponding expression derived by Landau and Lifshitz (1987) but with inverted indices.

We next consider the Newtonian limit of $(\tilde{v}_{12})_{SR}$ which is obtained when both $c_s(p_3) \ll 1$

and $c_s(p_1) \ll 1$. In this case,

$$\begin{aligned} A_+(p_3) &\simeq \left(1 - \frac{c_s(p_3)}{\sqrt{\gamma-1}}\right)^{4/\sqrt{\gamma-1}} \left(1 + \frac{c_s(p_1)}{\sqrt{\gamma-1}}\right)^{4/\sqrt{\gamma-1}} \\ &\simeq \left(1 - \frac{4c_s(p_3)}{\gamma-1}\right) \left(1 + \frac{4c_s(p_1)}{\gamma-1}\right) \\ &\simeq 1 - \frac{4}{\gamma-1}(c_s(p_3) - c_s(p_1)). \end{aligned} \quad (8.2)$$

so that the Newtonian limit of $(\tilde{v}_{12})_{SR}$ is given by

$$\begin{aligned} (\tilde{v}_{12})_{SR} \Big|_{\text{Newt}} &= \frac{1 - A_+(p_3)}{2} \Big|_{p_3=p_2} \\ &\simeq -\frac{2}{\gamma-1}c_s(p_1) \left[1 - \frac{c_s(p_3)}{c_s(p_1)}\right] \Big|_{p_3=p_2}. \end{aligned} \quad (8.3)$$

Bearing in mind that

$$\frac{c_s(p_3)}{c_s(p_1)} \Big|_{p_3=p_2} = \left(\frac{p_2}{p_1}\right)^{(\gamma-1)/2\gamma}, \quad (8.4)$$

we obtain

$$(\tilde{v}_{12})_{SR} \Big|_{\text{Newt}} = -\frac{2}{\gamma-1}c_s(p_1) \left[1 - \left(\frac{p_2}{p_1}\right)^{(\gamma-1)/2\gamma}\right], \quad (8.5)$$

which again coincides with the corresponding expression derived by Landau and Lifshitz (1987) but with inverted indices.

Finally, we consider the Newtonian limit of $(\tilde{v}_{12})_{2R}$ for $c_s(p_1), c_s(p_2) \ll 1$. In this case

$$\begin{aligned} S_1 &\simeq 1 + \frac{4c_s(p_1)}{\gamma-1}, \\ S_2 &\simeq 1 - \frac{4c_s(p_2)}{\gamma-1}. \end{aligned} \quad (8.6)$$

so that the Newtonian limit is given by

$$\begin{aligned} (\tilde{v}_{12})_{2R} \Big|_{\text{Newt}} &= \frac{S_2 - S_1}{S_1 + S_2} = \left[-\frac{4c_s(p_1)}{\gamma-1} - \frac{4c_s(p_2)}{\gamma-1} \right] \left[2 + \frac{4}{\gamma-1}[c_s(p_1) - c_s(p_2)] \right]^{-1} \\ &= \left[-\frac{2c_s(p_1)}{\gamma-1} - \frac{2c_s(p_2)}{\gamma-1} \right] \left[1 - \frac{2}{\gamma-1}[c_s(p_1) - c_s(p_2)] \right] \\ &= -\frac{2c_s(p_1)}{\gamma-1} - \frac{2c_s(p_2)}{\gamma-1}. \end{aligned} \quad (8.7)$$

Once more, expression (8.7) coincides with the corresponding expression derived by Landau and Lifshitz (1987) but with inverted indices.

Appendix C: A closed form solution in the case of Two Rarefaction Waves

As discussed in Sections 6 and 7, when $(\tilde{v}_{12})_{2R} < (v_{12})_0 < (\tilde{v}_{12})_{SR}$, the initial conditions give rise to two rarefaction waves and it is possible to derive a closed form solution for the unknown pressure p_* . In this way we can, at least in principle, avoid any numerical root finding procedure and determine the solution exactly. In this Appendix we first derive this analytic solution in the

context of relativistic hydrodynamics and then calculate its Newtonian limit. We will restrict ourselves to considering the particular case of a polytropic equation of state (2.2).

Using expression (3.4) we can write the pressures p_3 and $p_{3'}$ as functions of the sound speeds $c_s(p_3)$ and $c_s(p_{3'})$ which, for convenience, we will hereafter refer to as x and x' respectively

$$p_3 = k_1^{-1/(\gamma-1)} \left[\frac{x^2(\gamma-1)}{\gamma(\gamma-1) - \gamma x^2} \right]^{\gamma/(\gamma-1)}, \quad (8.1)$$

$$p_{3'} = k_2^{-1/(\gamma-1)} \left[\frac{(x')^2(\gamma-1)}{\gamma(\gamma-1) - \gamma(x')^2} \right]^{\gamma/(\gamma-1)}, \quad (8.2)$$

where $k_1 = p_1/\rho_1^\gamma$ and $k_2 = p_2/\rho_2^\gamma$ are the two constants entering the polytropic equation. Since $p_3 = p_{3'} = p_*$, we can obtain the following relation between x' and x :

$$(x')^2 \equiv \frac{\gamma(\gamma-1)x^2}{\gamma x^2(1-\alpha) + \alpha\gamma(\gamma-1)}, \quad (8.3)$$

where $\alpha \equiv (k_1/k_2)^{1/\gamma}$. The expression for the relative velocity (6.4) can also be written as

$$\frac{A_+(p_3)}{A_-(p_{3'})} = \frac{1 - (v_{12})_0}{1 + (v_{12})_0}. \quad (8.4)$$

and we then use expressions (5.2) and (6.3) to expand the left hand side of (8.4). After some algebra we are then left with

$$\left(\frac{\Gamma - x}{\Gamma + x} \right) \left(\frac{\Gamma - x'}{\Gamma + x'} \right) = \left[\frac{\Gamma - c_s(p_2)}{\Gamma + c_s(p_2)} \right] \left[\frac{\Gamma - c_s(p_1)}{\Gamma + c_s(p_1)} \right] \left[\frac{1 - (v_{12})_0}{1 + (v_{12})_0} \right]^{\Gamma/2}, \quad (8.5)$$

where $\Gamma^2 \equiv \gamma - 1$ and the right hand side of (8.5) is a constant which we rename as

$$\Pi \equiv \left[\frac{\Gamma - c_s(p_2)}{\Gamma + c_s(p_2)} \right] \left[\frac{\Gamma - c_s(p_1)}{\Gamma + c_s(p_1)} \right] \left[\frac{1 - (v_{12})_0}{1 + (v_{12})_0} \right]^{\Gamma/2}. \quad (8.6)$$

Introducing now the auxiliary quantity

$$\beta \equiv \frac{1 + \Pi}{1 - \Pi}, \quad (8.7)$$

expression (8.5) can be written as

$$(x')^2 = \left[\frac{\Gamma(x\beta - \Gamma)}{x - \Gamma\beta} \right]^2. \quad (8.8)$$

Comparing now (8.3) and (8.8) gives a 4-th order equation in the unknown sound velocity x

$$a_0 x^4 + a_1 x^3 + a_2 x^2 + a_3 x + a_4 = 0, \quad (8.9)$$

where

$$a_0 \equiv 1 - \beta^2(1 - \alpha), \quad (8.10)$$

$$a_1 \equiv -2\Gamma\alpha\beta, \quad (8.11)$$

$$a_2 \equiv \Gamma^2(1 - \alpha)(\beta^2 - 1), \quad (8.12)$$

$$a_3 \equiv 2\Gamma^3\alpha\beta, \quad (8.13)$$

$$a_4 \equiv -\alpha\Gamma^4. \quad (8.14)$$

The analytic solution of equation (8.9) will yield at least two real roots, one of which will be the physically acceptable one: i.e. positive, less than one, and such that the pressure p_* falls in the relevant bracketing interval.

In its Newtonian limit, equation (8.9) reduces to a second order equation in the unknown sound velocity

$$\left(\frac{1}{\alpha} - 1\right)x^2 + 2\Sigma x - \Sigma^2 = 0, \quad (8.15)$$

where

$$\Sigma \equiv c_s(p_1) + c_s(p_2) + \frac{(\gamma - 1)}{2}v_{12}, \quad (8.16)$$

and $v_{12} = v_1 - v_2$. The fact that the Newtonian Riemann problem in the case of two rarefaction waves can be solved analytically is well known and is at the basis of the so called ‘‘Two Rarefaction Approximate Riemann Solver’’ (Toro 1997).

REFERENCES

- COLELLA, P. AND WOODWARD, P. R. 1984, The Piecewise Parabolic Method (PPM) for Gas-Dynamical Simulations, *J. Comput. Phys.*, **54**, 174.
- COURANT, R. AND FRIEDRICHS, K. O. 1948, *Supersonic Flows and Shock Waves*, Interscience.
- GHELLER, C. 1997, A High Resolution Hydrodynamical Code for the Study of Cosmological Structures, *PhD Thesis*, SISSA.
- GODUNOV, S. K. 1959, A Finite Difference Method for the Numerical Computation and Discontinuous Solutions of the Equations of Fluid Dynamics, *Mat. Sb.*, **47**, 271.
- IBAÑEZ, J.M. & MARTÍ, J.M. 1999, Riemann Solvers in Relativistic Astrophysics, *J. Comput. Appl. Math.*, in press.
- LANDAU, L. D. AND LIFSHITZ, E. M. 1987, *Fluid Mechanics (Second Edition)*, Pergamon.
- MARTÍ, J.M. & MÜLLER, E. 1994, The Analytical Solution of the Riemann Problem in Relativistic Hydrodynamics, *J. Fluid Mech.*, **258**, 317.
- MARTÍ, J.M. & MÜLLER, E. 1996, Extension of the Piecewise Parabolic Method to One-Dimensional Relativistic Hydrodynamics, *J. Comput. Phys.* **123**, 1.
- MARTÍ, J.M. & MÜLLER, E. 1999 Numerical Hydrodynamics in Special Relativity, *Living Reviews in General Relativity*, astro-ph/9906333.
- PONS, J.A., FONT, J.A., MARTÍ, J.M., IBAÑEZ, J.M. & MIRALLES, J.A. 1998, General Relativistic Hydrodynamics with Special Relativistic Riemann Solvers, *Astron. Astroph.* **339**, 638.
- PONS, J.A., MARTÍ, J.M., MÜLLER, E. 2000, The exact solution of the Riemann problem with non zero tangential velocities in relativistic hydrodynamics *J. Fluid Mech.* **422**, 125.
- ROE, P. L. 1981, Approximate Riemann Solvers, Parameter Vectors and Difference Scheme, *J. Comp. Phys.*, **43**, 357.
- SOD, G. A. 1978, A Survey of Several Finite Difference Methods for Systems of Nonlinear Hyperbolic Conservation Laws, *J. Comp. Phys.*, **27**, 1.
- TAUB, A. H., 1948, Relativistic Rankine-Hugoniot Relations, *Phys. Rev.*, **74**, 328.
- TAUB, A. H., 1978, Relativistic Fluid Mechanics, *Ann. Rev. Fluid Mech.*, **10**, 301.
- TORO, E. 1997, *Riemann Solvers and Numerical Methods for Fluid Dynamics*, Springer.